

1 **Synchrony of trend shifts in Sahel boreal summer rainfall and global oceanic**
2 **evaporation, 1950–2012**

3

4 **A. Diawara¹, Y. Tachibana¹, K. Oshima², H. Nishikawa¹ and Y. Ando¹**

5 [1]{Weather and Climate Dynamics Division, Mie University, Tsu, Japan}

6 [2]{Institute of Arctic Climate and Environment Research, Japan Agency for Marine-Earth
7 Science and Technology, Yokosuka, Japan}

8 Correspondence to: Yoshihiro Tachibana (tachi@bio.mie-u.ac.jp)

9

10 **Abstract**

11 Between 1950 and 2012, boreal summer (rainy season) rainfall in the Sahel changed from a
12 multi-decadal decreasing trend to an increasing trend (positive trend shift) in the mid-1980s. We
13 found that this trend shift was synchronous with similar trend shifts in global oceanic
14 evaporation and in land precipitation in all continents except the Americas. The trend shift in
15 oceanic evaporation occurred mainly in the southern hemisphere (SH) and the subtropical oceans
16 of the northern hemisphere (NH). Because increased oceanic evaporation strengthens the
17 atmospheric moisture transport toward land areas, the synchrony of oceanic evaporation and land
18 precipitation is reasonable. Surface scalar winds over the SH oceans also displayed a positive
19 trend shift. Sea surface temperature (SST) displayed a trend shift in the mid-1980s that was
20 negative (increasing, then decreasing) in the SH and positive in the NH. Although SST had
21 opposite trend shifts in both hemispheres, the trend shift in evaporation was positive in both
22 hemispheres. We infer that because strong winds promote evaporative cooling, the trend shift in
23 SH winds strengthened the trend shifts of both SST and evaporation in the SH. Because high
24 SST promotes evaporation, the trend shift in NH SST strengthened the NH trend shift in
25 evaporation. Thus differing oceanic roles in the SH and NH generated the positive trend shift in
26 evaporation; however, the details of moisture transport toward the Sahel are still unclear or
27 perhaps there is no single determining influence.

28

29 **1 Introduction**

30 For the past sixty years, the West African Sahel region, located between 10°N – 20°N
31 longitude, has been one of the most important research areas for studying climatic variability due
32 to its fragile climate conditions. While there are many well-documented analyses of the Sahel's
33 drought conditions since the early 1970s (e.g., Hulme, 1992, Christensen et al., 2007, Baines and
34 Folland, 2007), there is no general explanation on the source of the drought. Several studies have
35 also shown that the Indian Ocean, the North and South Atlantic Ocean, and the southern
36 hemisphere (SH) oceans and the Mediterranean Sea have, alone or together, some kind of remote
37 influence on the distribution of Sahel rainfall (Palmer, 1986; Giannini et al., 2003; Wolter, 1989;
38 Janicot et al., 1996; Rowell, 2003; Hagos and Cook, 2008; Diatta and Fink, 2014). Studies and
39 evaluations of the Sahel monsoon are crucial to determine previous precipitation variations,
40 provide climate projections, and offer a scientific response to the decrease in rainfall over the
41 majority of the region (Dai et al., 2001, Omotosho et al., 2008); however, the exact linkage
42 between the multi-decadal variations of the Sahel rainfall and the global ocean remain unclear.
43 Sahel rainfall is correlated with remote SST, which suggests that global-scale ocean evaporation
44 processes are potentially important for the historical land surface rainfall variability. Our initial
45 analysis suggested that the global hydrological cycle is comprised of evaporation from some part
46 of the ocean surface and the transport of water vapor over the African continent. Therefore, it is
47 reasonable that moisture transport from different parts of the world ocean may, either alone or in
48 combination, affect African precipitation in general and that of the Sahel in particular.

49 Some of the earliest works related to nearby sea surface temperatures (SSTs) have shown
50 that precipitation time's series have significantly changed over the last sixty years (Lough, 1986;
51 Bader and Latif, 2003; Chung and Ramanathan, 2006). Other studies related to remote SST point
52 out that the precipitation time's series has considerably changed over that the past sixty years as
53 well (Folland et al., 1986; Janicot et al., 1996; Rowell, 2003; Fontaine et al., 2011; Munemoto
54 and Tachibana, 2012; Diatta and Fink, 2014). The potential long-term causes and effects of SST
55 variability are important inputs for the thermo-dynamical process of Sahel rainfall (Folland et al.
56 1986; Giannini et al. 2003; Tippett & Giannini 2006; Lu and Delworth 2005; Hoerling et al.
57 2006). Although long-term climate trends are commonly related to the state of the ocean, the
58 radiative forcing by changing levels of greenhouse gas and/or aerosols have been considered

59 responsible for the changes of climate in the global ocean and on each continent except
60 Antarctica (Stott et al., 2010). Yet, the increased trend of the greenhouse gas has not been linked
61 to the trend shift of the Sahel rainfall. Delworth et al. (1993) defined the thermal impacts of the
62 North Atlantic thermohaline overturning flow at multi-decadal scales. Zhang and Delworth
63 (2006) referred to the subsequent SST pattern as the Atlantic Multi-decadal Oscillation. Pomposi
64 et al. (2015) examined the role of global SST anomalies and their effects on monsoon variability
65 in the Sahel region and found that “much of the internal variability of the global monsoon
66 system” is generated by SST variances and their outcome on the atmospheric teleconnections,
67 linking oceanic variations to land-based rainfall. Munemoto and Tachibana (2012) demonstrated
68 that the contrast between North and South SST also corresponds to the more recent pattern of
69 Sahel rainfall; in the mid-1980s, the phenomenon shifted from a decreasing trend to an
70 increasing trend. These various studies underscore the lack of a single mechanism determining
71 the relationship between the shift of the Sahel rainfall and the shift of oceanic evaporation.
72 Folland et al. (1986) were among the first to historically establish a relationship between Sahel
73 rainfall and (SH) SST on multi-decadal time scales; this relationship has demonstrated that when
74 the SH SST is higher (lower) than normal, the Sahel is drier (wetter) than normal (Folland et al.,
75 1986). Bader and Latif (2003) considered the warming trend in the Indian Ocean to have “a
76 crucial role for the [forty-year] drying trend over the West Sahel.” As a consequence, Indian
77 Ocean warming may have contributed to the strengthening of the North Atlantic Oscillation
78 during these last two decades. In addition, their experiments highlight the influence of the
79 tropical Pacific over the eastern Sahel, whereas the tropical Atlantic influences rainfall only over
80 the Atlantic itself and along the western Sahel.

81 For this study, we analyzed global evaporation datasets for the second half of the 20th
82 century in order to determine whether the previously established linkages between remote SST
83 and Sahel rainfall are the result of remote linkages between Sahel rainfall and oceanic
84 evaporation. We also investigated the underlying trends in wind stress and SST that may explain
85 changes in evaporation. Given the region’s exposure to natural variability, favoring severe
86 drought with unexplained sequence variations, this study will deliver a skillful multi-decadal
87 climate forecast for the Sahel.

88

89 2 Data and Methods

90 For the precipitation, we used 3 different monthly datasets: from 1949 to 2014, the National
91 Oceanic and Atmospheric Administration (NOAA) Precipitation Reconstruction over Land
92 (PREC/L) database (Chen et al., 2002) with a spatial resolution of 1.0 degree in latitude and
93 longitude; the Global Precipitation Climatology Centre (GPCC) data (Schneider et al. 2011),
94 2.5x2.5, from 1949 to 2013; and the University of Delaware UDel_AirT_Precip data provided by
95 the NOAA/OAR/ESRL PSD, Boulder, Colorado, USA, from their Web site at
96 <http://www.esrl.noaa.gov/psd/>, resolution of 0.5x0.5 and from 1949 to 2013. For SST, we used
97 monthly data from 1953 to 2012 in the NOAA Extended Reconstructed SST Version 3 (NOAA
98 ERSST V3) dataset, which is constructed from SST data in the International Comprehensive
99 Ocean-Atmosphere Data Set (ICOADS) (Smith et al., 2008; Xue et al., 2003). Monthly 10-m
100 scalar wind speed data from 1950 to 2011 came from Wave and Anemometer-based Sea Surface
101 Wind (WASWind) version 1.0.1 (Tokinaga and Xie, 2011), derived from ship observations in
102 ICOADS and presented at a resolution of 4×4 degrees. Specific humidity data at 2-degree
103 resolution was from ICOADS. Both wind speed and specific humidity databases have missing
104 values in areas outside shipping routes, especially at high latitudes. Because Chiu et al. (2012)
105 view oceanic evaporation, or sea surface latent heat flux (LHF) divided by the latent heat of
106 vaporization (L_v), as a crucial factor of the global water and energy cycle, we used LHF data for
107 1950–2012 from the National Centers for Environmental Prediction/National Center for
108 Atmospheric Research (NCEP/NCAR) Reanalysis (Kalnay et al., 1996) as a fundamental proxy
109 for oceanic evaporation. We also used data from the Japanese Re-Analysis 55 Years (JRA-55)
110 (Kobayashi et al., 2015) and the European Centre for Medium-Range Weather Forecasts
111 (ECMWF) 40-year Reanalysis (ERA-40) (Uppala et al., 2005) datasets and compared these
112 datasets to the LHF data from NCEP/NCAR and the moisture flux vector. Based on the
113 comparison, we addressed possible reliability problems in moisture data from the pre-satellite era.
114 Although there are some differences between these three databases, the differences do not
115 significantly influence our conclusions. Our analysis primarily used July-August-September
116 (JAS) averages, corresponding to the Sahel region's rainy season.

117 Figure 1 shows the long-term value of JAS average precipitation in northern Africa using
118 PREC_L data. Our study area, defined as the region bounded by 10°N - 20°N and 8°W - 30°E , was
119 chosen to avoid coastal influences on seasonal rainfall in the Sahel. The JAS has captured, by

120 definition, the Sahel region rainy season between 200 to 600 mm per JAS per year and we used
121 the PREC_L data for the smooth resolution of the data. Figure 2 shows the variation of JAS
122 average rainfall in the study area from 1950 through 2012. Sahel rainfall decreased from the
123 early 1960s to the mid-1980s, followed by an increasing trend for the rest of the study period.
124 The driest year of the study period was 1984 (Munemoto and Tachibana, 2012); we focused on
125 that period to divide our dataset into two different periods, the decreasing and increasing periods.
126 The mid-1980s mark a clear reversal in these multi-decadal trends. The signature of this trend
127 shift is not sensitive to the definition of the study area (results not shown). Because the data were
128 insufficient to analyze at least two cycles of multi-decadal variability, we focused on a
129 phenomenon ("the trend shift") that might indicate a phase change.

130 To assess the degree to which trends in other climatic parameters synchronized with the
131 Sahel trend shift, we divided the time series of all datasets into the subperiods 1950–1984 and
132 1985–2012. We defined the trend in each subperiod as the angle of inclination, $\tan\theta$, of the time
133 series, as calculated from the linear regression coefficient using the least squares method. We
134 defined the strength of the trend shift, $\delta\tan\theta$, as $\tan\theta_2 - \tan\theta_1$, where the subscripts 1 and 2
135 denote the subperiods before and after 1984, respectively. To confirm that the trends of the two
136 subperiods differed in sign, we added the condition $\tan\theta_1 \cdot \tan\theta_2 < 0$. We named a decreasing to
137 increasing (increasing to decreasing) trend shift as a positive (negative) trend shift, i.e., $\delta\tan\theta >$
138 0 ($\delta\tan\theta < 0$) and $\tan\theta_1 \cdot \tan\theta_2 < 0$.

139

140 **3 Results**

141 **3.1 Trend shifts of Sahel precipitation and ocean evaporation**

142 The time series of the global JAS mean LHF decreased before the mid-1980s, followed by
143 an increase (Figure 2). Although this increase ceased after the mid-1990s, the turning point of the
144 trend shift coincided with Sahel rainfall. Global annual mean LHF also had a similar trend shift
145 to that of the JAS mean (Li et al., 2011). This synchrony suggests that, at the multi-decadal time
146 scale, the variability of Sahel rainfall may be physically linked to the transport of the moisture
147 flux from the oceans. We also investigated global mean sensible heat flux, but found no
148 significant trends during the study period.

149 The trend shift of LHF in the world ocean may be related to precipitation inside and outside
150 the Sahel. The results of our investigation of this possibility are shown for both JAS and annual
151 precipitation of PREC_L in Figure 3a and 3b, respectively. The trend shift over the Sahel is
152 stronger for annual precipitation than for JAS precipitation. The areas where the positive trend
153 shifts (from decreasing to increasing) in JAS precipitation are large are the Sahel, western coastal
154 areas of South Asia, and equatorial South America (Figure 3a).

155 For annual precipitation, the areas with positive trend shifts are more numerous than the
156 areas with negative trend shifts (Figure 3b). Positive trend shifts are particularly strong in the
157 Sahel, western coastal areas of South Asia, and southern Chile and less strong in Korea, Japan,
158 the Philippines, Alaska, and northern Eurasia. Negative trend shifts are seen in South America,
159 most of the SH, most of North America, and inland Eurasia; these areas are weaker and narrower
160 than the areas with a positive trend shift. These results indicate that a positive trend shift in
161 precipitation occurred not only in the Sahel but elsewhere in the globe. Comparing the trend
162 shifts of JAS precipitation of the PREC_L (Figure 3a), GPCC (Figure 3c), and the University of
163 Delaware (Figure 3d) datasets, similar land coverage was observed, with a correlation of 0.9;
164 however, the University of Delaware (Figure 3d) dataset showed a weaker signal over the same
165 areas included in the PREC_L and GPCC datasets.

166

167 **3.2 Global SST trend shift**

168 Sahel rainfall is related to nearby SST (Lough, 1986, Bader and Latif, 2003; Chung and
169 Ramanathan, 2006) and remote SST (Folland et al., 1986; Janicot et al., 1996; Rowell, 2003;
170 Fontaine et al., 2011; Munemoto and Tachibana, 2012; Diatta and Fink, 2014). Although there is
171 not visible evidence of change, it is conceivable that the SST time series has a changing phase
172 from 1984 using the SST over the northern hemisphere (NH) and SH. As demonstrated by
173 Munemoto and Tachibana (2012), the NH SST became lower than that of the SH SST and
174 described an opposite trend after 1984. Figure 4 shows that areas of positive trend shift in the
175 JAS SST over the oceans are widespread in the NH, meaning that SST decreased until 1984 and
176 then increased. Areas of negative trend shift are mostly in the SH, particularly the eastern
177 tropical Pacific and the South Atlantic Ocean. The obvious contrast between hemispheres

178 suggests that the change in JAS Sahel rainfall is somehow related to the hemispheric contrast in
179 SST; these results are consistent with the findings of Folland et al. (1986) and Munemoto and
180 Tachibana (2012). In addition, modeling and observational studies by Bader and Latif (2003)
181 show that the Sahel region rainfall variability is linked with regional and global SST anomaly
182 patterns, which include fluctuations in: the tropical Atlantic Ocean, as pointed out by Lamb
183 (1978), Hastenrath, (1984), and Lamb and Pepler, (1992); the Pacific Ocean, as alluded by
184 Janicot et al. (1996) and Rowell (2001); the Indian Ocean, as referred to by Palmer (1986) and
185 Shinoda and Kawamura (1994); and the Mediterranean, as mentioned by Rowell (2003).

186 **3.3 Trend shift of global ocean evaporation**

187 The time change of the SST, i.e., SST trend, should be linearly related to the evaporation
188 from the ocean provided that the ocean is treated as a slab. The time change of the evaporation,
189 i.e., LHF trend, should thus be linearly related to the second-order differential of the SST. Here
190 we simply compare between the two trend shifts, because the quality of the global dataset dose
191 not resolve the second-order differential. Figure 5a and b show the JAS trend shift's geographic
192 distribution of land water vapor flux and global ocean evaporation, as defined by LHF using
193 NCEP and JRA-55 data, respectively. They both show a similar signs over the oceans, except at
194 the coastline of western South America and the tropical Atlantic; one possible explanation is that
195 the JRA-55 data are missing at least 10 years before 1984, which could capture the tropical
196 Atlantic magnitude. When the subtropical SH Atlantic ocean is warmer (colder) than normal,
197 greater (lesser) LHF production is observed, with a deeper surface coverage of the moisture flux
198 transient through the western coast of the Sahel region, whereas the NCEP data show coverage
199 transient through the eastern Sahel coast; similar results were found by Bader and Latif (2003).
200 The NCEP and JRA-55 datasets captured a significant relation over the Sahel region, even
201 though the JRA-55 evaporation rate increases at the western side of Sahel region and is negative
202 in the eastern part. The relation of the tropical Pacific ocean, El Nino, and both the northern and
203 southern Atlantic with the Sahel's rainfall variation, which was confirmed by Zhang et al. (2006),
204 is observed in the JRA-55 data, but not the the NCEP/NCAR data.

205

206 **3.4 Trend shifts of wind, humidity**

207 Latent heat flux is determined by surface wind speed and the humidity deficit over the ocean.
208 As displayed on Figure 6, the trend shift of JAS surface scalar wind speeds over the ocean. This
209 shift is positive over most of the SH, particularly in the eastern Pacific Ocean. Many of these
210 positive areas match areas with positive LHF trend shifts (Figure 5). In the NH, the trend shift is
211 positive over the subtropical central and eastern Pacific. Over the western subtropical North
212 Atlantic ocean, the trend shift in the scalar wind is not in agreement with the trend shift in LHF;
213 nevertheless, the overall similarity of Figure 6 and Figure 5 signifies that trend shifts in wind
214 speed over the ocean partially account for the trend shift in LHF.

215 The trend shift in the JAS deficit of surface specific humidity, as determined from its
216 saturated value at the local SST, is shown in Figure 7. The geographic distribution of this
217 positive trend shift is essentially global, similar to those of SST (Figure 4) and LHF (Figure 5) in
218 the NH and the southern Pacific Ocean. The positive trend shift of global evaporation from the
219 ocean is therefore also partially explained by this trend shift.

220 Figure 8 shows a map of the JAS moisture flux trend shift using JRA-55. On this figure we
221 can observe anticyclonic curvature from the eastern tropical Pacific toward tropical Atlantic;
222 eastward flux from the tropical Atlantic to the Sahel region; the flux from Indian Ocean in about
223 40S trough the South Atlantic Ocean is also witnessed. This flux is further connected to the
224 tropical Atlantic Ocean. Most importantly, this figure clearly highlights the key role the South of
225 Indian Ocean and the East of the Pacific Ocean play in Sahel rainfall variation. In addition, a
226 weaker transport from the North Atlantic through Mediterranean Ocean entrance to Libya is also
227 observed, however this phenomenon is blocked by the local high pressure located in the Sahara
228 desert.

229

230 **4 Discussion and conclusion**

231 Our study demonstrates an important synchrony between Sahel rainfall and global
232 evaporation from oceans. The key point is that the shift in the trend of JAS Sahel rainfall from
233 decreasing to increasing (positive trend shift) occurred in the mid-1980s and coincided with
234 shifts in global-scale SST and evaporation from the oceans (Table 1). We found that the Sahel

235 trend shift was synchronous with similar positive trend shifts in global oceanic evaporation
236 (Figure 2) and in land precipitation outside the Sahel, except in the Americas (Figure 3). In detail,
237 the trend shift in oceanic evaporation (as indicated by LHF) encompassed the SH and the
238 subtropical NH, including the Pacific, Atlantic, and Indian Oceans (Figure 5). Because increased
239 oceanic evaporation strengthens global moisture transport toward the land, the synchronization
240 of these trend shifts is physically plausible, and indeed the area of increased LHF exceeded the
241 area of decreased LHF. Trend shifts also occurred in the mid-1980s in SST: the shift was
242 negative (increase to decrease) in the SH and positive in the NH, giving rise to an
243 interhemispheric contrast in SST (Figure 4). The surface scalar wind over the ocean had a
244 positive trend shift, mainly in the SH, that extended to the subtropical Pacific Ocean in the NH
245 (Figure 6). The humidity deficit displayed a positive trend shift in both hemispheres, particularly
246 in the Pacific Ocean (Figure 7). The strongest statement comes from the vector moisture flux,
247 which clearly represents the path of the moisture flux from the eastern Pacific and South Indian
248 Oceans through the tropical southern Atlantic to the western entrance of the Sahel region, and
249 also the tropical northern Atlantic through northern Europe through Libya as an entrance that
250 was, however, dissipated by the blocked high pressure in the Sahara region (Figure 8). The
251 eastern Pacific and South Indian Oceans are the areas where the positive trend shift of the latent
252 heat flux is observed (Figure 5)

253 From these results, we can assert that the process that connects the trend shifts of the global
254 oceans and Sahel rainfall is summarized in Figure 9, which is the main reason for the positive
255 trend shift in LHF, is the positive trend shift in scalar wind, particularly in the SH, because
256 surface wind promotes evaporation from the ocean. When SST is greater than normal, the
257 atmosphere becomes unstable, leading to an interaction between convection and large-scale
258 circulation that strengthens the convergence at the surface with a low wind speed at this center,
259 generating a small amount of latent heat flux. LHF lowers the SST due to evaporative cooling,
260 which was also suggested by Wu et al. (2009) and Zhang et al. (1994). Therefore, the negative
261 trend shift in SH SST may be an effect of the positive trend shift in the scalar wind. Giannini et
262 al. (2003) and Zeng (2003) demonstrated that in the SH, when the gulf is warm, the Intertropical
263 Convergence Zone (ITCZ) shifts south away from the Sahel, reducing the African monsoon that
264 draws moist air into the Sahel, which means that long-term changes in Sahel rainfall are induced
265 by changes in SST in the tropical Atlantic and Pacific oceans. The opposite way is that the

266 advection of the magnitude of the moisture flux from the oceans toward the Sahel region forces
267 the ITCZ to shift northward toward the Sahel region during the boreal summer. Although the
268 linkages can be viewed as speculative and conceptual, the phenomenon could explain why both
269 hemispheres are correlated positively, even though their SSTs are different.

270 In the NH, at latitudes lower than 40°N, the LHF trend shift tended to be positive, in
271 synchrony with the positive SST trend shift. Because high SST in low latitudes generally
272 promotes evaporation, the positive trend shift in LHF may be a consequence of the positive trend
273 shift in SST; the positive trend shift in the humidity deficit in the NH also supports this inference.
274 Thus, the positive SST trend shift in the NH may be linked to the positive LHF trend shift.
275 Although the trend shift in SST is positive in the NH and negative in the SH, hemispheric
276 differences in the role of SST may result in a global positive trend shift in LHF.

277 Although our study offers an explanation for these global-scale trend shifts, the reason for the
278 outsized signature of Sahel rainfall is still problematic. In line with our viewpoint, Pomposi et al.
279 (2015) affirmed that “understanding of how the monsoon reacts to global SSTs remains
280 incomplete because the system can be impacted by moisture availability locally and in the region
281 as well as tropical atmospheric stability, both of which are influenced by ocean temperatures.” In
282 the past, the influence of SST in different remote sites was emphasized (Folland et al., 1986;
283 Czaja and Frankignoul, 2002; Dijkstra, 2006; Ting et al., 2009), including in the Atlantic Ocean
284 (Hu and Huang, 2006; Marullo et al., 2011; Martin et al., 2014), Pacific Ocean (Rowntree, 1972;
285 Pan and Oort, 1983; Cayan and Peterson, 1989; Wallace et al., 1989), and Indian Ocean
286 (Clemens et al., 1991; Ashok et al., 2001, 2003; Annamalai et al., 2005). To identify how
287 evaporation in these remote oceans drives Sahel rainfall, idealized atmospheric general
288 circulation model studies will need to incorporate the anomalous SST patterns shown in this
289 study. The processes underlying the trend shift of the ocean surface wind also must be identified.
290 Additionally, it is noteworthy that the trend shift in oceanic evaporation might affect the global
291 salinity distribution, and in turn the global thermohaline circulation. Remarkably, the SST-Sahel
292 teleconnection seems to be stronger with the Indian Ocean (negative correlation) and
293 Mediterranean index (positive correlation) in about 50% of the years of that era (Fontaine et al.,
294 2011), which led us to conclude that the resemblance between global trends and trends in the
295 Sahel makes it difficult to attribute changes in the Sahel to only a single teleconnection. Largely,

296 the horizontal transfer of heat flux from oceans to the Sahel region through precipitation
297 variability (or opposite) has been highlighted.

298 Furthermore, our experiments confirm the hypothesis that the south Indian Ocean, east
299 Pacific Ocean, and Atlantic Ocean significantly influence not only regional climate anomalies, as
300 Bader and Latif (2003) suggested, but also the relationship between global changes in SSTs and
301 the Sahel region's rainfall variability, as revealed by Folland et al. (1986). The conclusion, which
302 one can draw from these various studies, is that the Sahel constitutes the world's largest area in
303 which this trend shift occurred. Rainfall or dry conditions in the West African Sahel region can
304 definitely be associated with the role of the global oceans.

305

306 **Acknowledgements**

307 We thank the Ministry of Education, Culture, Sports, Science and Technology (MEXT) for
308 the opportunity afforded by the international student scholarship program. MEXT supported this
309 study through a Grant-in-Aid for Scientific Research on Innovative Areas (Grant Number
310 22106003). We extend special thanks to Kunihiko Kodera, Koji Yamazaki and Nicholas
311 Heavens for insightful discussions. We also thank the editor and anonymous reviewers for their
312 valuable comments and suggestions to improve the quality of the paper. The Grid Analysis and
313 Display System (GrADS) and Generic Mapping Tools (GMT) were used to draw the figures.

314

315 **References**

316 Annamalai, H., Liu, P., and Xie, S. P.: Southwest Indian Ocean SST Variability Its Local Effect
317 and Remote Influence on Asian Monsoons, *J. Climate*, 18, 4150–4167, doi: 10.1175/JCLI3533.1,
318 2005.

319 Ashok, K., Guan, Z., and Yamagata, T.: Impact of the Indian Ocean dipole on the relationship
320 between the Indian Monsoon rainfall and ENSO, *Geophys. Res. Lett.*, 28, 4499–4502,
321 doi:10.1029/2001GL013294, 2001.

322 Ashok, K., Guan, Z., and Yamagata, T.: Influence of the Indian Ocean Dipole on the Australian
323 winter rainfall, *Geophys. Res. Lett.*, 30, 1821-1825, doi:10.1029/2003GL017926, 2003.

324 Bader, J. and Latif, M.: The impact of decadal-scale Indian Ocean sea surface temperature
325 anomalies on Sahelian rainfall and the North Atlantic Oscillation, *Geophys. Res. Lett.*, 30, 2169-
326 2172, doi:10.1029/2003GL018426, 2003.

327 Baines, P. G., and Folland, C. K.: Evidence for rapid global climate shift across the late 1960s, *J.*
328 *Climate*, 20, 2721 – 2744, doi:10.1175/JCLI4177.1, 2007.

329 Cayan, D. R. and Peterson, D. H.: The Influence of North Pacific Atmospheric Circulation on
330 Streamflow in the West, in *Aspects of Climate Variability in the Pacific and the Western*
331 *Americas*, *Geophys. Monogr.*, No. 55, *Amer. Geophys. Union*, 375–397,
332 doi:10.1029/GM055p0375, 1989.

333 Chen, M., Xie, P., Janowiak, J. E., and Arkin, P. A.: Global Land Precipitation: A 50-yr
334 Monthly Analysis Based on Gauge Observations, *J. Hydrometeor.*, 3, 249-266, 2002.

335 Chiu L.S, Gao S. and Shie C-L: *Oceanic Evaporation: Trends and Variability*, p261, 2012.

336 Christensen, J.H., Hewitson, B., Busuioc, A., Chen, A., Gao, X. Held, I., Jones, R., Kolli, R.
337 K., Kwon, W.-T., Laprise, R., Rueda, V. M., Mearns, L., Menéndez, C.G., Räisänen, J., Rinke,
338 A., Sarr, A., and Whetton, P.: Regional Climate Projections. In: *Climate Change 2007: The*
339 *Physical Science Basis. Contribution of Working Group I to the Fourth Assessment Report of*
340 *the Intergovernmental Panel on Climate Change* [Solomon, S., D. Qin, M. Manning, Z. Chen,
341 M. Marquis, K.B. Averyt, M. Tignor and H.L. Miller (eds.)]. Cambridge University Press,
342 Cambridge, United Kingdom and New York, NY, USA, 2007.

343 Chung, C. E. and Ramanathan, V.: Weakening of North Indian SST Gradients and the Monsoon
344 Rainfall in India and the Sahel, *J. Climate*, 19, 2036–2045, doi:10.1175/JCLI3820.1, 2006.

345 Clemens, S., Prell, W., Murray, D., Shimmiel, G., and Weedon, G.: Forcing mechanisms of the
346 Indian Ocean monsoon. *Nature*, 353, 720-725, doi:10.1038/353720a0, 1991.

347 Czaja, A. and Frankignoul, C.: Observed Impact of Atlantic SST Anomalies on the North
348 Atlantic Oscillation, *J. Climate*, 15, 606–623, doi:10.1029/2004JD005676, 2002.

349 Dai, A.: Drought under global warming: a review, *WIREs Climate Change*, 2, 45-65,
350 doi:10.1002/wcc.81, 2011.

351 Delworth, T. L., Manabe, S., and Stouffer, R. J.: Interdecadal variations of the thermohaline
352 circulation in a coupled ocean-atmosphere model, *J. Climate*, 6, 1993 – 2010, doi:10.1175/1520-
353 0442(1993)006<1993:IVOTTC>2.0.CO;2, 1993.

354 Diatta, S. and Fink, A. H.: Statistical relationship between remote climate indices and West
355 African monsoon variability, *Int. J. Climatol.*, 34-12, 3348-3367, doi:10.1002/joc.3912, 2014.

356 Dijkstra, H. A.: Interaction of SST Modes in the North Atlantic Ocean, *J. Phys. Oceanogr.*, 36,
357 286–299, doi:10.1175/JPO2851.1, 2006.

358 Folland, C. K., Palmer, T. N., and Parker, D. E.: Sahel rainfall and worldwide sea temperatures,
359 1901-85, *Nature*, 320, 602-607, doi:10.1038/320602a0, 1986.

360 Fontaine, B., Gaetani, M., Ullmann, A., and Roucou, P.: Time evolution of observed July–
361 September sea surface temperature-Sahel climate teleconnection with removed quasi-global
362 effect (1900–2008), *J. Geophys. Res.*, 116, D04105, doi:10.1029/2010JD014843, 2011.

363 Giannini, A., Saravanan, R., and Chang, P.: Oceanic forcing of Sahel rainfall on annually to
364 interdecadal time scales, *Science*, 302, 1027–1030, doi:10.1126/science.1089357, 2003.

365 Hagos, S. M. and Cook, K. H.: Ocean Warming and Late-Twentieth-Century Sahel Drought and
366 Recovery, *J. Climate*, 21, 3797-3814, doi:10.1175/2008JCLI2055.1, 2008.

367 Hastenrath, S.: Interannual Variability and Annual Cycle: Mechanisms of Circulation and
368 Climate in the Tropical Atlantic Sector, *Mon. Weather Rev.*, 112, 1097-1107, doi:10.1175/1520-
369 0493(1984)112<1097:IVAACM>2.0.CO;2, 1984.

370 Hoerling, M., J. Hurrell, Eischeid, J. and Phillips, A.: Detection and attribution of 20th century
371 northern and southern African rainfall change, 19, 3989-4008, *J. Climate*, 2006.

372 Hu, Z. Z. and Huang, B.: Physical Processes Associated with the Tropical Atlantic SST
373 Meridional Gradient, *J. Climate*, 19, 5500–5518, doi:10.1175/JCLI3923.1, 2006.

374 Hulme M.: Rainfall changes in Africa: 1931–1960 to 1961–1990. *Int. J. Climatol.* 12: 685–699,
375 1992.

376 Janicot, S., Moron, V., and Fontaine, B.: Sahel droughts and ENSO dynamics, *Geophys. Res.*
377 *Lett.*, 23, 515–518, doi:10.1029/96GL00246, 1996.

378 Kalnay E., Kanamitsu, M., Kistler, R., Collins, W., Deaven, D., Gandin, L., Iredell, M., Saha, S.,
379 White, G., Woollen, J., Zhu, Y., Cheillab, M., Ebsuzaki, W., Higgins, W., Janowiak, J., Mo, K.
380 C., Ropelewski, C., Wang, J., Leetma, A., Reynolds, P., Jenne, R., and Joseph, D.: The
381 NCEP/NCAP 40-year reanalysis project, *B. Am. Meteorol. Soc.*, 77, 437-470, 1996.

382 Kobayashi, S., Ota, Y., Harada, Y., Ebata, A., Moriya, M., Onoda, H., Onogi, K., Kamahori, H.,
383 Kobayashi, C., Endo, H., Miyaoka, K., and Takahashi, K.: The JRA-55 Reanalysis: General
384 Specifications and Basic Characteristics, *J. Meteorol. Soc. Jpn*, 93, 5-48, doi:10.2151/jmsj.2015-
385 001, 2015.

386 Lamb, P. J., and R. A. Pepler: Further Case Studies of Tropical Atlantic Surface Atmospheric
387 and Oceanic Patterns Associated with Sub-Saharan Drought, *J. Climate*, 5, 476-488,
388 doi:10.1175/1520-0442(1992)005<0476:FCSOTA>2.0.CO;2, 1992.

389 Lamb, P. J.: Large-scale Tropical Atlantic surface circulation patterns associated with
390 Subsaharan weather anomalies. *Tellus*, 30, 240-251, 1978.

391 Li, G., B. Ren, J. Zheng, and C. Yang: Trend singular value decomposition analysis and its
392 application to the global ocean surface latent heat flux and SST anomalies, *J. Climate*,
393 doi:10.1175/2010JCLI3743.1, 2011.

394 Lough, J. M.: Tropical Atlantic Sea Surface Temperatures and Rainfall Variations in Subsaharan
395 Africa, *Mon. Weather. Rev.*, 114, 561–570, doi:10.1175/1520-
396 0493(1986)114<0561:TASSTA>2.0.CO;2, 1986.

397 Lu, J., and T. Delworth: Oceanic forcing of the late 20th century Sahel drought. *Geophys. Res.*
398 *Lett.*, 32, L22706, doi:10.1029/2005GL023316, 2005.

399 Martin, E. R., Thorncroft, C., and Booth, B. B.: The Multidecadal Atlantic SST—Sahel Rainfall
400 Teleconnection in CMIP5 Simulations, *J. Climate*, 27, 784–806, doi:10.1175/JCLI-D-13-
401 00242.1, 2014.

402 Marullo, S., Artale, V., and Santoleri, R.: The SST Multidecadal Variability in the Atlantic–
403 Mediterranean Region and Its Relation to AMO, *J. Climate*, 24, 4385–4401,
404 doi:10.1175/2011JCLI3884.1, 2011.

405 Munemoto, M. and Tachibana, Y.: The recent trend of increasing precipitation in Sahel and the
406 associated inter-hemispheric dipole of global SST, *Int. J. Climatol.*, 32, 1346–1353,
407 doi:10.1002/joc.2356, 2012.

408 Omotosho, J. B.: Pre-rainy season moisture build-up and storm precipitation delivery in the West
409 African Sahel. *Int. J. Climatol.*, 28 937–946, 2008.

410 Palmer, T. N.: Influence of the Atlantic, Pacific and Indian Oceans on Sahel rainfall, *Nature*, 322,
411 251-253, doi:10.1038/322251a0, 1986.

412 Pan, Y. H. and Oort, A. H.: Global Climate Variations Connected with Sea Surface Temperature
413 Anomalies in the Eastern Equatorial Pacific Ocean for the 1958–73 Period, *Mon. Weather. Rev.*,
414 111, 1244–1258, doi:10.1175/1520-0493(1983)111<1244:GCVCWS>2.0.CO;2, 1983.

415 Rowell, D. P.: The Impact of Mediterranean SSTs on the Sahelian Rainfall Season, *J. Climate*,
416 16, 849–862, doi:10.1175/1520-0442(2003)016<0849:TIOMSO>2.0.CO;2, 2003.

417 Rowell, D. P.: Teleconnections between the tropical Pacific and the Sahel. *Q. J. R. Meteorol.*
418 *Soc.*, 127, 1683–1706, 2001.

419 Rowntree, P. R.: The influence of tropical east Pacific Ocean temperatures on the atmosphere, *Q.*
420 *J. R. Meteorol. Soc.*, 98, 290–321, doi:10.1002/qj.49709841605, 1972.

421 Schneider, U., Becker, A., Finger, P., Meyer-Christoffer, A., Rudolf, B., and Ziese, M.: GPCP
422 Full Data Reanalysis Version 6.0 at 2.5°: Monthly Land-Surface Precipitation from Rain-Gauges
423 built on GTS-based and Historic Data, doi: 10.5676/DWD_GPCP/FD_M_V7_250, 2011.

424 Shinoda, M., and Kawamura, R.: Tropical rainbelt, circulation, and sea surface temperatures
425 associated with the Sahelian rainfall trend. *J. Meteor. Soc. Japan*, 72, 341-357, 1994.

426 Smith, T. M., Reynolds, R. W., Peterson, T. C., and Lawrimore, J.: Improvements to NOAA's
427 Historical Merged Land-Ocean Surface Temperature Analysis (1880-2006), *J. Climate*, 21,
428 2283–2296, 2008.

429 Stott, P. A., Gillett, N. P., Hegerl, G. C., Karoly, D. J., Stone, D. A., Zhang, X., and Zwiers, F.:
430 Detection and attribution of climate change: A regional perspective, *Wiley Interdiscip. Rev.*
431 *Clim. Change*, 1, 192-211, 2010.

432 Ting, M., Kushnir, Y., Seager, R., and Li, C.: Forced and Internal Twentieth-Century SST
433 Trends in the North Atlantic, *J. Climate*, 22, 1469–1481, doi:10.1175/2008JCLI2561.1, 2009.

434 Tippet, M., and Giannini, A.: Potentially predictable components of African summer rainfall in
435 an SST-forced GCM simulation, *J. Climate*, 19, 3133–3144, 2006.

436 Tokinaga, H. and Xie, S. P.: Wave and Anemometer-based Sea Surface Wind (WASWind) for
437 Climate Change Analysis, *J. Climate*, 24, 267-285, doi:10.1175/2010JCLI3789.1, 2011.

438 Uppala and co-authors : The ERA-40 re-analysis, *Q. J. R. Meteorol. Soc.*, 131, 2961–3012,
439 doi:10.1256/qj.04.176, 2005.

440 Wallace, J. M., Mitchell, T. P., and Deser, C.: The Influence of Sea-Surface Temperature on
441 Surface Wind in the Eastern Equatorial Pacific: Seasonal and Interannual Variability, *J. Climate*,
442 2, 1492–1499, doi:10.1175/1520-0442(1989)002<1492:TIOSST>2.0.CO;2, 1989.

443 Wolter, K.: Modes of tropical circulation, Southern Oscillation, and Sahel rainfall anomalies, *J.*
444 *Climate*, 2, 149-172, doi:10.1175/1520-0442(1989)002<0149:MOTCSO>2.0.CO;2, 1989.

445 Wu R., Kirtman, B. P., and Pegion, K.: Surface latent heat flux and its relationship with sea
446 surface temperature in the National Centers for Environmental Prediction Climate Forecast
447 System simulation and retrospective forecasts, *Geophys. Res. Lett.*, 34, L17712,
448 doi:10.1029/2007GL030751, 2009.

449 Xue, Y., Smith, T. M., and Reynolds, R. W.: Interdecadal changes of 30-yr SST normals during
450 1871-2000, *J. Climate*, 16, 1601-1612, doi:10.1175/1520-0442-16.10.1601, 2003.

451 Zhang, R., and Delworth, T. L.: Impact of Atlantic multidecadal oscillations on India/Sahel
452 rainfall and Atlantic hurricanes, *Geophys. Res. Lett.*, 33, L17712, doi:10.1029/2006GL026267,
453 2006.

454 Zeng, N.: Drought in the Sahel, *Science*, 302, 999–1000, 2003.

455 Zhang G.,J, and Mcphaden M. J.: The relationship between sea surface temperature and latent
456 heat flux in the equatorial Pacific, *J. Climate*, 8(3), 589–605, 1995.

457 Table 1. Summary of Results for JAS Meteorological Parameters. “Positive” indicates that a shift
 458 from decrease to increase occurred during 1950 to 2012; “negative” indicates a shift from
 459 increase to decrease.

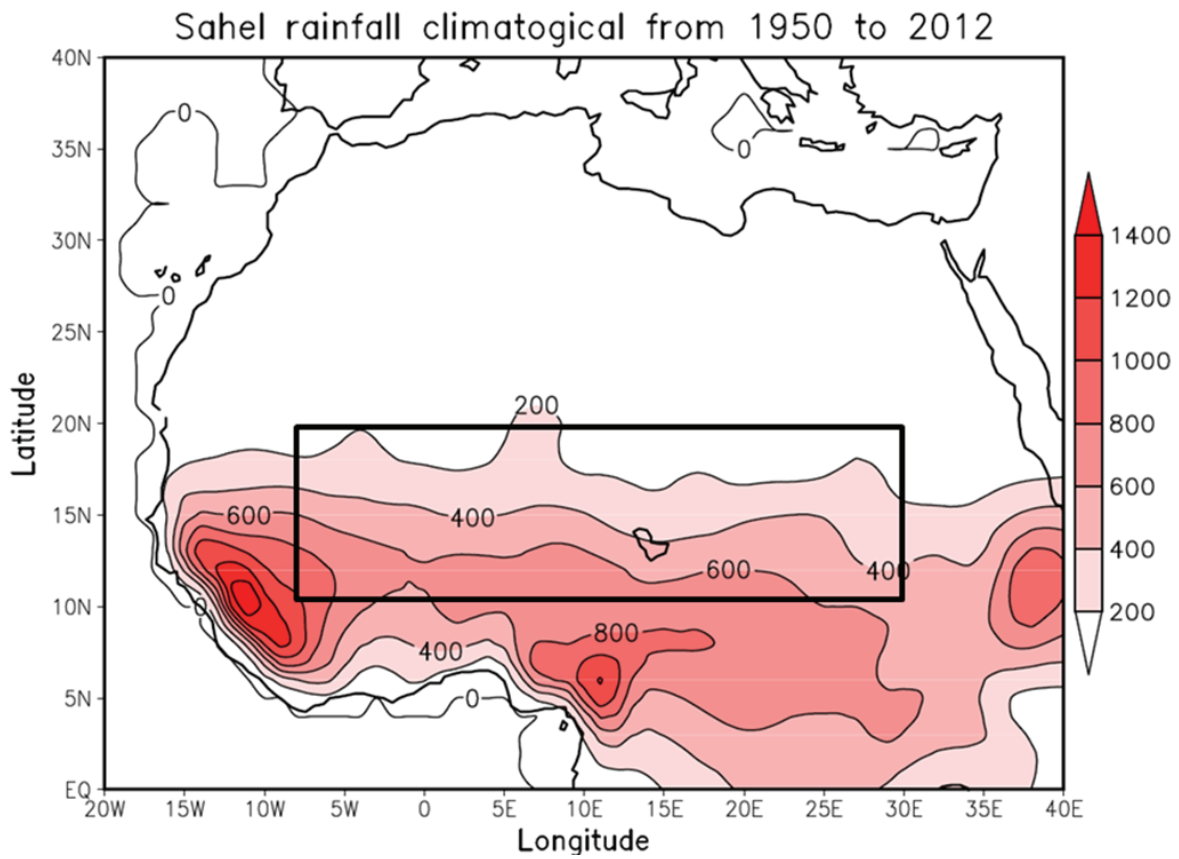
460

	Sahel rain	SST	LHF	Wind	Humidity deficit
Northern hemisphere	Positive	Positive	Positive	Positive (tropical Pacific)	Positive
Southern hemisphere		Negative	Positive	Positive	Positive (Pacific)

461

462

463



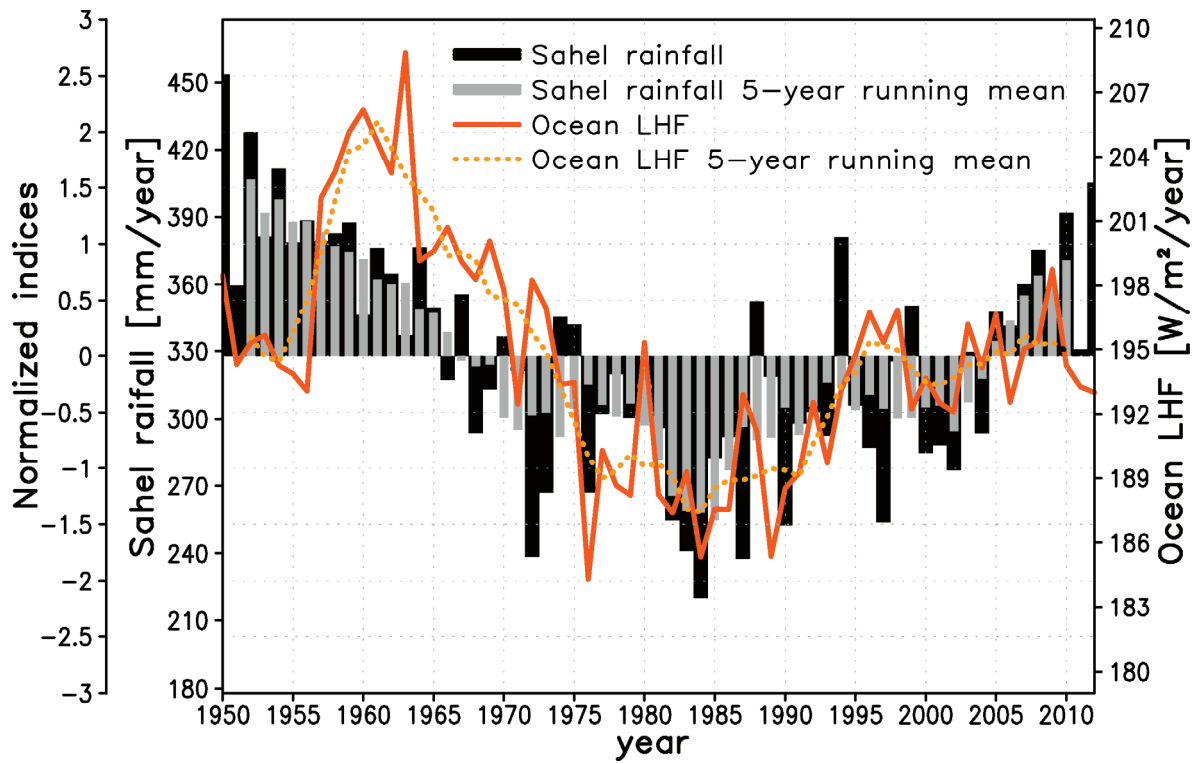
464

465 Figure.1 Climatological JAS mean of North Africa region rainfall averaged from 1950 to 2012.
466 The area defined as the Sahel region is in the rectangle between latitude 10-20°N and longitude
467 8°W-30°E. The unit is mm.

468

469

470



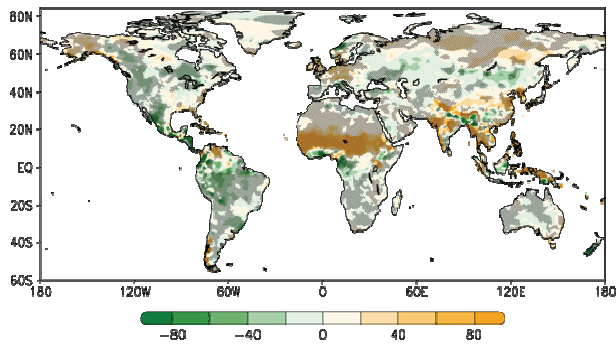
471

472

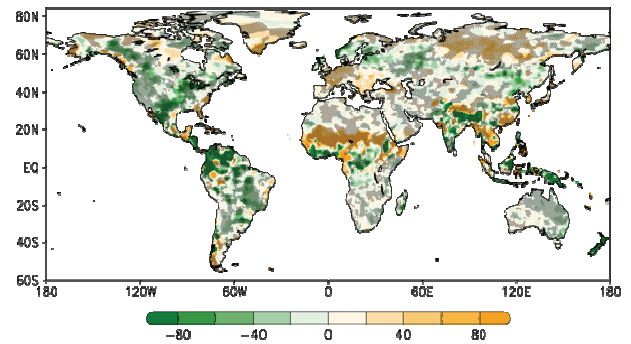
473 Figure 2. Time series of JAS Sahel rainfall (mm) and mean LHF ($W m^{-2}$) from oceans from
 474 1950 to 2012.

475

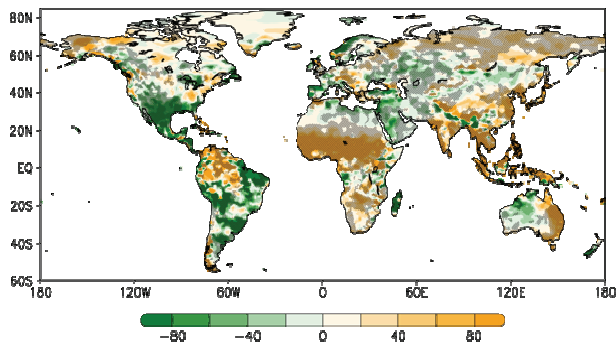
(a) JAS-PREC_L



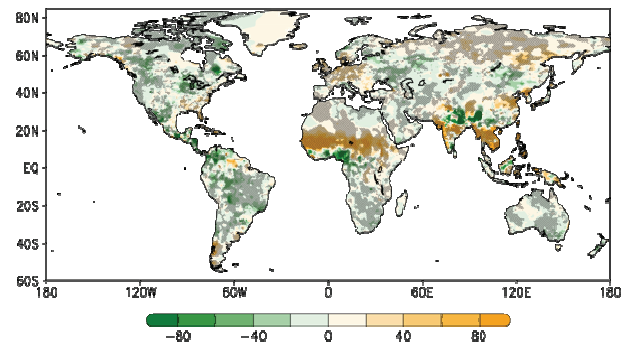
(c) JAS-GPCC



(b) Annual-PREC_L



(d) JAS-University of Delaware

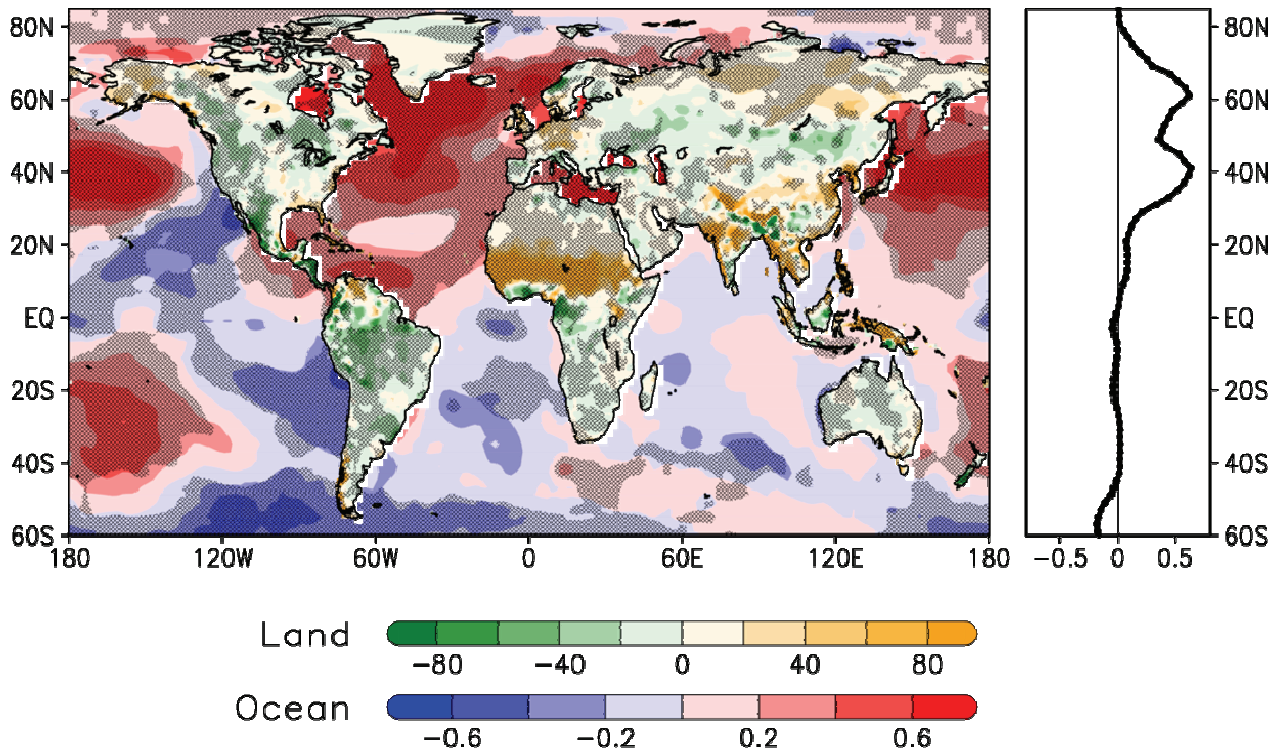


476

477 Figure 3. Global maps of the trend shift for (a) JAS precipitation PREC_L ($\text{mm } 10\text{years}^{-1}$), (b)
478 annual precipitation, (c) JAS precipitation GPCC and (d) JAS precipitation University of
479 Delaware. Shading denotes $\delta \tan \theta$. Hatching represents areas where trends changed sign
480 between the two parts of the study period ($\tan \theta_1 \cdot \tan \theta_2 < 0$).

481

482



483

484 Figure 4. (Left) Trend shifts in SST (K/10years) and (Right) latitude profile of its zonal mean.
 485 Land areas display trend shifts in JAS precipitation from Figure 3a. Hatching represents areas
 486 where trends changed sign between the two parts of the study period ($\tan\theta_1 \cdot \tan\theta_2 < 0$).

487

488

489

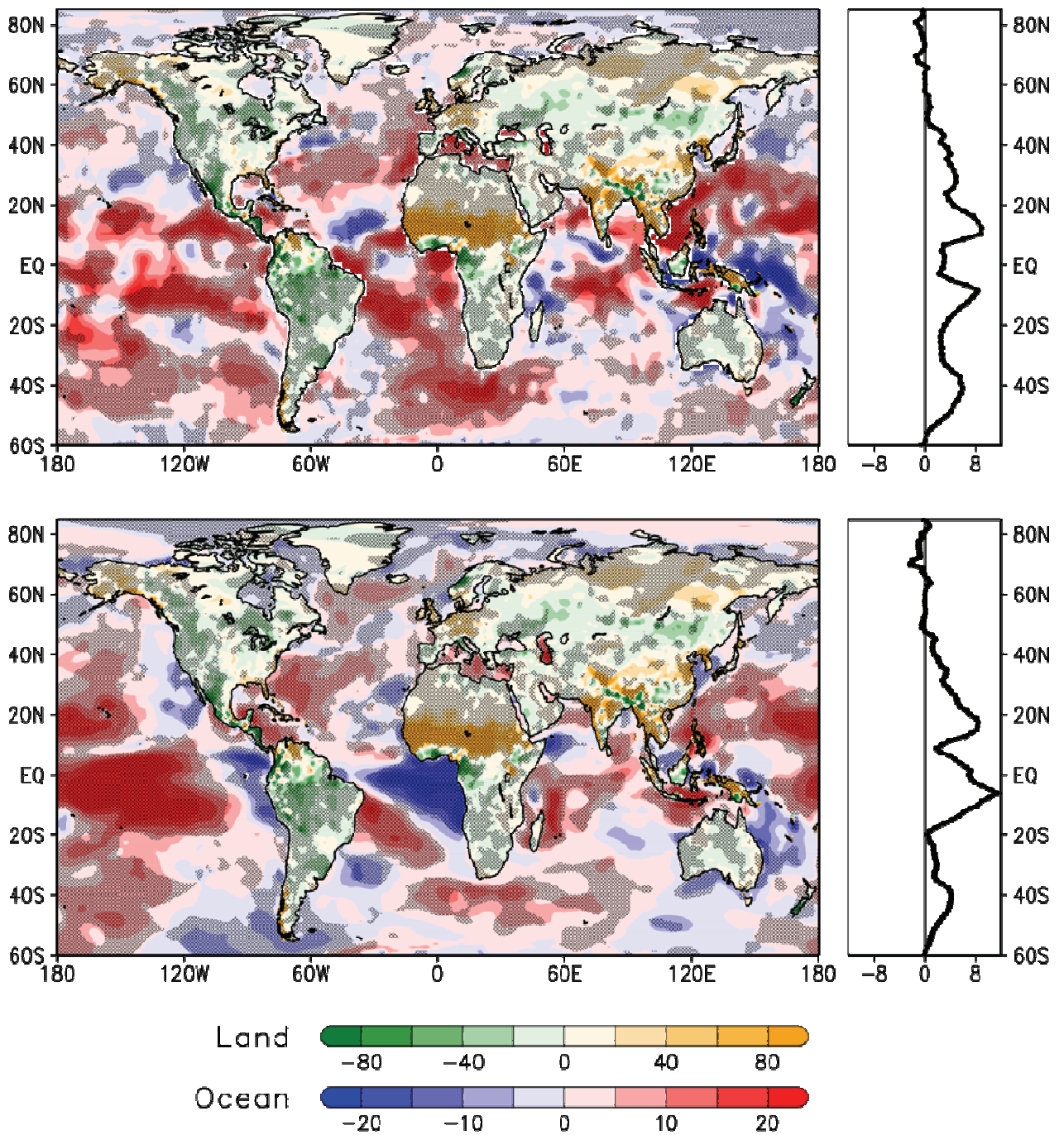
490

491

492

493

494

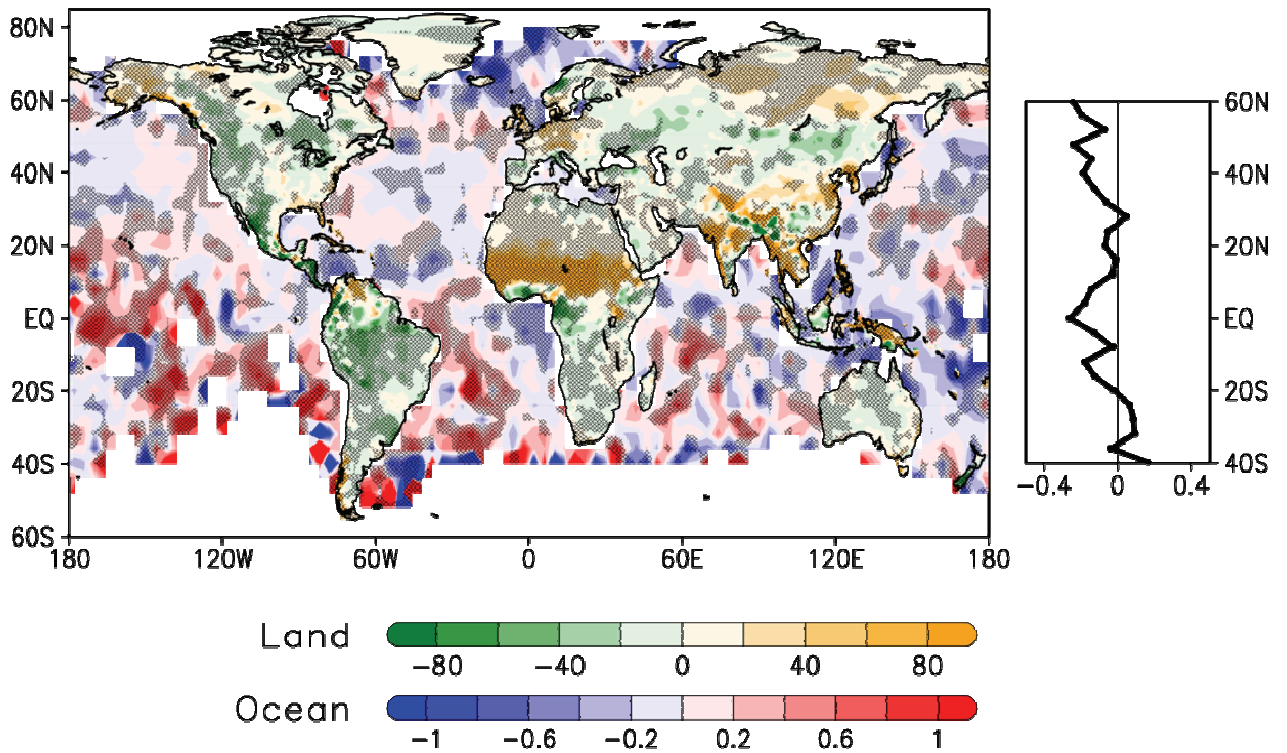


495

496 Figure 5. Global maps of the LHF trend shift over the oceans for (a) JAS-NCEP ($\text{W m}^{-2}/10\text{years}$) and (b) JAS-JRA55. Land areas display trend shifts in JAS precipitation from Figure
 497 3a. Shading denotes $\delta \tan \theta$. Hatching represents areas where trends changed sign between the
 498 two parts of the study period ($\tan \theta_1 \cdot \tan \theta_2 < 0$).
 499

500

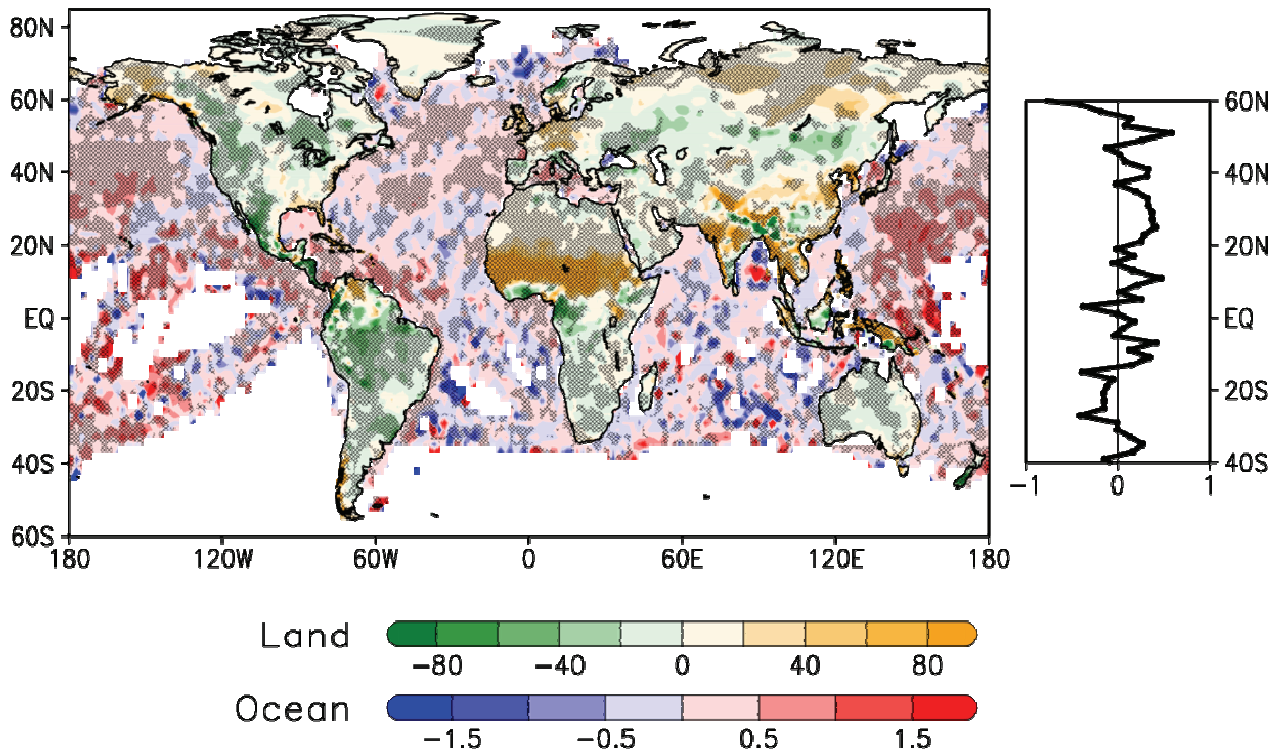
501



502

503 Figure 6. (Left) Trend shifts in scalar wind speed over the ocean (m s⁻¹/10years) and (Right)
504 latitude profile of its zonal mean. Land areas display trend shifts in JAS precipitation from
505 Figure 3a. Hatching represents areas where trends changed sign between the two parts of the
506 study period ($\tan\theta_1 \cdot \tan\theta_2 < 0$).

507



508

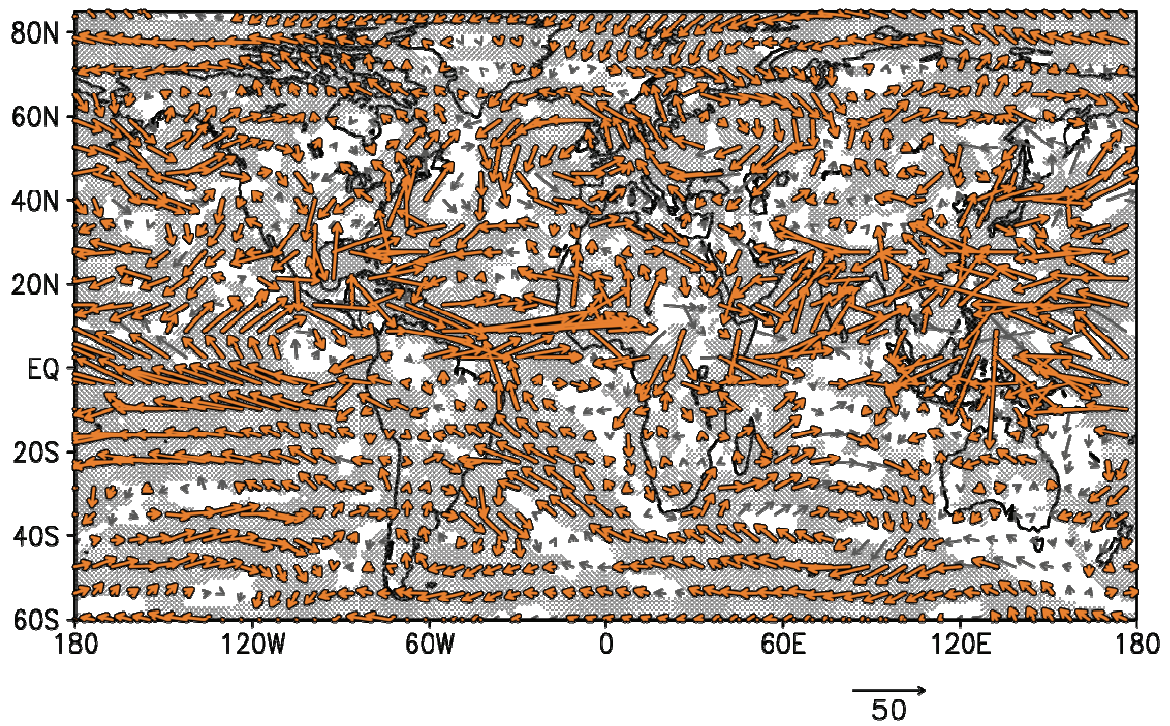
509

510 Figure 7. (Left) Trend shifts in the humidity deficit ($\text{g kg}^{-1}/10\text{years}$) over the ocean and (Right)
 511 latitude profile of its zonal mean. Land areas display trend shifts in JAS precipitation from
 512 Figure 3a. Hatching represents areas where trends changed sign between the two parts of the
 513 study period ($\tan\theta_1 \cdot \tan\theta_2 < 0$).

514

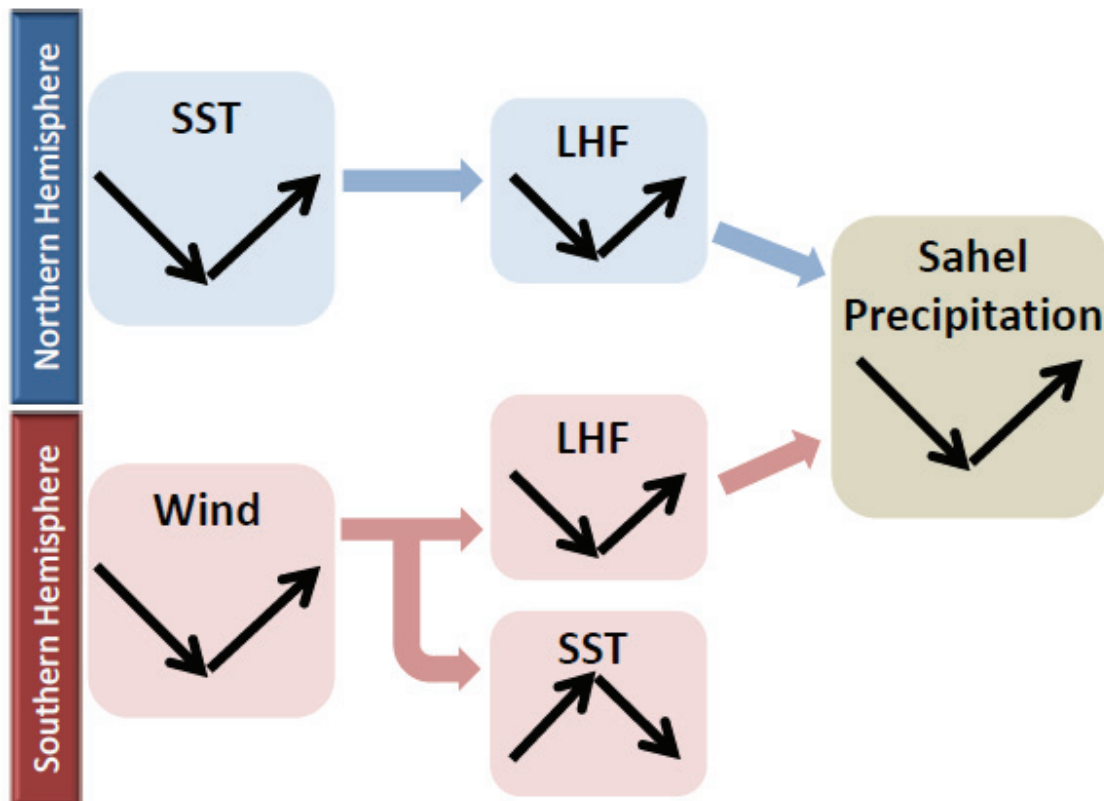
515

516



517

518 Figure 8. Trend shift vector map of moisture flux using JRA-55 ($\text{kg m}^{-1} \text{s}^{-1}/10\text{years}$), 1958-2014:
 519 JAS). Orange bold vector and hatching represent areas where northward or eastward moisture
 520 flux trends changed sign between the two parts of the study period ($\tan\theta_1 \cdot \tan\theta_2 < 0$).



521

522 Figure 9. Schematic diagram of possible processes linking Sahel precipitation and the global
 523 ocean. The arrows represent increases or decreases in a parameter during 1950–1984 and 1985–
 524 2012.

525

526